ELSEVIER

Polymer 44 (2003) 1391–1399

polymer

www.elsevier.com/locate/polymer

Polyimide/montmorillonite nanocomposites based on thermally stable, rigid-rod aromatic amine modifiers

Zhu-Mei Liang, Jie Yin*, Hong-Jie Xu

Research Institute of Polymer Materials, School of Chemistry and Chemical Technology, State Key Lab of Composite Materials, Shanghai Jiao Tong University, Shanghai 200240, People's Republic of China

Received 7 October 2002; received in revised form 7 November 2002; accepted 9 December 2002

Abstract

The preparation and processing of most of polymer/clay nanocomposites need high temperature. This limited the application of commonly used organic modifiers of long carbon-chain alkyl ammonium salts because of their low thermal stability. In this study, we synthesized two novel thermally stable, rigid-rod aromatic amines. Montmorillonite (MMT) treated by these amines exhibited larger layer-to-layer spacing, higher thermal stability than that treated by commonly used 1-hexadecylamine and also high ion-exchange ratio (>95%). They were applied to prepare nanocomposites with polyimide (PI) by in situ polymerization. XRD, TEM were used to obtain the information on morphological structure of PI/MMT nanocomposites. DMA, TGA, DSC, universal tester were applied to characterize the mechanical and thermal properties of the nanocomposites. When the MMT content was below 3 wt%, the PI/MMT nanocomposites were strengthened and toughened at the same time. The introduction of a small amount of MMT also led to improvement in thermal stability, slight increase in glass transition temperature, marked decrease in coefficient of thermal expansion and decrease in solvent uptake. MMT treated by these aromatic amines exhibited better dispersibility and (probably) interfacial interaction with PI matrix than that treated by 1-hexadecylamine. The nanocomposites based on these MMT resultantly exhibited better mechanical, thermal and solvent resistance properties than those based on 1-hexadecylamine treated MMT.

Keywords: Montmorillonite; Nanocomposites; Polyimide

1. Introduction

Polymer/inorganic nanocomposites based on the intercalation of polymer chains into organically modified layered silicates (OLS) form a class of nanocomposites that have recently received considerable attention [1–25], because they often exhibit superior physical, mechanical and thermal properties to conventional mineral-filled composites or unfilled polymers. These performance improvements depend greatly on the distribution, arrangement of OLS and synergism between the layered silicate and the polymer.

Clay is a type of layered silicate, and the most commonly used clay in the preparation of polymer/clay nanocomposites is montmorillonite (MMT). MMT is composed of silicate sheets of about 1 nm thickness with adsorbed exchangeable alkali or alkaline earth cations such as Na^+, K^+, Ca^{2+}. Before the preparation of polymer/MMT nanocomposites, modification is generally required through ion exchange reaction between organic cations and inorganic cations to render hydrophilic MMT more organophilic and to increase interlayer spacing of MMT, aiming at providing a better physical and chemical environment for the polymer.

The commonly used organo-modification agents are long carbon-chain alkyl ammonium salts. It has been widely accepted that the interlayer spacing of OLSs depends greatly on the length of the carbon chain [1]. Although these modification agents have been gaining significant success in the preparation of polymer/MMT nanocomposites, their common shortcoming is the poor thermal stability. Xie et al. [20,21] have studied the thermal stability of MMT modified by long carbon-chain alkyl quaternary ammonium ions using TGA-MS and found that the on-set decomposition temperature of the resultant OLSs was approximately

* Corresponding author. Tel.: +86-21-54743269; fax: +86-21-54741297.
E-mail address: jyin@sjtu.edu.cn (J. Yin).

0032-3861/03/$ - see front matter © 2003 Elsevier Science Ltd. All rights reserved.
PII: S0032-3861(02)00911-4

180 °C. Unfortunately, the preparation and processing of most of the polymer/OLS nanocomposites require a temperature much higher than this value, and the thermal decomposition of the long carbon-chain alkyl quaternary ammonium salts is inevitable. Delozier et al. [22] observed that during the preparation of polyimide/clay nanocomposites, the decomposition of the organic modifier led to the 'collapse of the clay particles into larger agglomerates'. This may affect the morphological structure, properties and service life of nanocomposites. Therefore, the thermal stability of organic modifier may pose significant effect on the preparation, performance and application of nanocomposites. However, little attention has been paid to improve thermal stability of the organic modifier while making nanocomposites so far.

Polyimide is considered to be one of the most important engineering plastics, and has outstanding mechanical and electrical properties, especially at elevated temperature, being an attractive candidate for many applications in electronics and photonics [29]. Recently, the studies on polyimide have been focused on the improvement in the mechanical properties, size stability and solvent resistance to satisfy its application field. The study on polyimide/MMT nanocomposites was first reported by Yano et al. [30,31]. Agag et al. [17] have studied polyimide/MMT nanocomposites based on BPDA/PDA and PMDA/ODA polyimide. Our group [24] has studied the morphology, solvent resistance and thermal properties of poly(etherimide)/MMT nanocomposites and found that the introduction of MMT led to an obvious decrease in the solvent uptake. These property improvements were based on the good dispersion of MMT and strong interaction between MMT and polyimide matrix. In all these studies, aliphatic amines were used as the modification agents. Very recently, works on the design of new structure organo-modifier have been reported [26,27].

In this paper, we report our study on the organo-modification of MMT using thermally stable aromatic amines. The amines contain thermally stable phenyl structure and imide moiety and, unlike aliphatic amines, have very rigid chemical structure (Scheme 1 (a) and (b)). These organo-modified MMTs were also used to prepare polyimide/MMT nanocomposites. They may possess better compatibility with aromatic polymers such as polyimide because of their structure similarity. Their properties were also studied.

2. Experimental

2.1. Materials

Sodium montmorillonite (Na-MMT) with a cation exchange capacity (CEC) of 100 meq/100 g was supplied by the Institute of Chemical Metallurgy, Chinese Academy of Sciences. The average particle size is 50 μm. *N*-[4-(4′-aminophenyl)]phenyl phthalimide (OM-l) and *N*-[4-(4′-aminophenoxy)]phenyl phthalimide (OM-m) were synthesized in our lab. 1-Hexadecylamine (OM-16C, $C_{16}H_{33}NH_2$, lab reagent) was purchased from Merck. 4,4′-Diamino-3, 3′-dimethyldiphenylmethane (MMDA) was synthesized by a reaction of *o*-methyl aniline with formaldehyde. Benzophenone-3,3′,4,4′-tetracarboxylic dianhydride (BTDA) was dehydrated from benzophenone-3,3′,4,4′-tetracarboxylic acid in acetic anhydride at reflux temperature. The solvent for the preparation of nanocomposites (*m*-cresol) was dried over molecular sieves before use. Other common reagents were used without further purification.

2.2. Synthesis of OM-l and OM-m

7.369 g (0.04 mol) 4,4′-diaminodiphenylether was dissolved in 50 ml dry N, *N*-dimethylacetamide (DMA). To it, a DMA solution (50 ml) of 5.924 g (0.04 mol) phthalic anhydride was added dropwise. The reaction was maintained for 5 h at room temperature, and then at refluxing temperature for 5 h. After cooling to room temperature, the product was precipitated from the reaction mixture. The green powdery primary product was collected by filtration and washed with 50 ml ethanol, and then purified by recrystallization with ethanol/*N*-methyl-2-pyrrolidone (NMP) (3/1) to obtain light green needle crystals. Yield: 9.876 g (74.1%). The synthesis of OM-m was followed by the procedure similar to that of OM-l. Yield: 9.545 g (68.5%). Elemental analysis (%): OM-l ($C_{20}H_{14}N_2O_2$), calc.: C, 76.43; H, 4.46; N, 8.92; found: C, 75.73; H, 4.72; N, 8.93. OM-m ($C_{20}H_{14}N_2O_3$), calc.: C, 72.73; H, 4.24; N, 8.48; found: C, 72.20; H, 4.56; N, 8.46. ^{1}H NMR analysis (400 MHz, $CDCl_3$, 20 °C): OM-l (δ, ppm): 7.96–6.76 (12H, phenyl): 7.96 (s, 2H), 7.79 (s, 2H), 7.64 (d, 2H), 7.44 (t, 4H), 6.76 (d, 2H), 2.20 (s, 2H, $-NH_2$). OM-m (δ, ppm): 7.94–6.70(12H, phenyl): 7.94(s, 2H), 7.78(s, 2H), 7.31(d, 2H), 7.03(d, 2H), 6.91(d, 2H), 6.70(d, 2H), 2.81 (s, 2H, $-NH_2$).

2.3. Preparation of organically modified MMT

The organically modified MMT was prepared via ion exchange reaction in water using OM-16C, OM-l and OM-m, respectively. For the preparation of MMT modified with OM-l (MMT-l), 1.08 g OM-l was mixed with 1 ml concentrated hydrochloric acid (37%) and 15 ml distilled water and heated at 80 °C for a few minutes, and to it was added a dispersion of 2.5 g Na-MMT in 100 ml distilled water. The mixture was stirred vigorously for 1 h at 80 °C. The white precipitate was filtered and washed repeatedly with hot water (80 °C) to remove the superfluous ammonium salts to be free from Cl^-. It was subsequently collected and dried in vacuum at 80 °C for 24 h. The preparation of MMT modified with OM-m (MMT-m) and OM-16C (MMT-16C) was followed by the procedure similar to that of MMT-l.

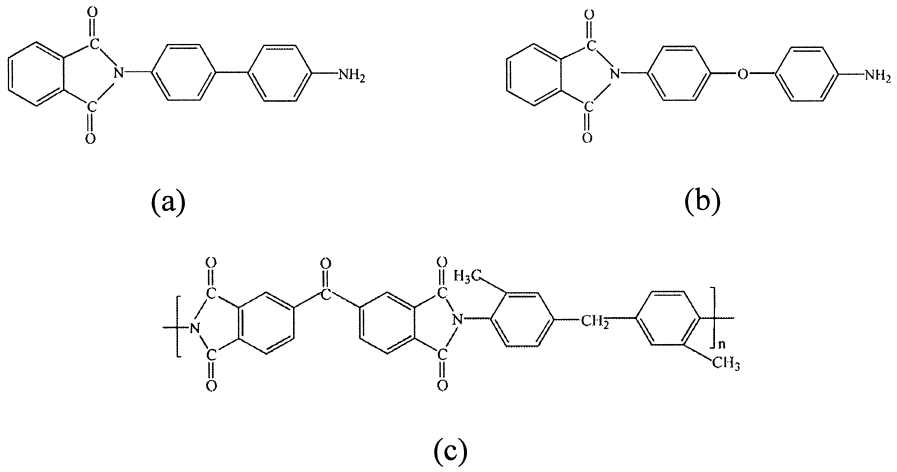

Scheme 1. Chemical structure of (a) OM-l, (b) OM-m and (c) polyimide.

2.4. Preparation of polyimide/MMT nanocomposites

The polyimide/MMT (PI/MMT) nanocomposites were prepared by an in situ polymerization approach. The modified MMT was thoroughly dispersed in 25 ml *m*-cresol with the help of vigorous stirring. To this dispersion, MMDA (1.130 g, 0.005 mol) and BTDA (1.610 g, 0.005 mol) and 3 drops of *iso*-quinoline were added, consecutively. The mixture was stirred vigorously at room temperature for 2 h and then heated at 180 °C for 3 h to obtain a yellow, transparent, highly viscous PI/MMT nanocomposite solution. It was used to cast thin films. The films were placed in a vacuum oven at room temperature for the removal of the air-bubble solutions, and then were thermally treated consecutively at 70 °C for 12 h, 120 °C for 4 h, 200 °C for 4 h, 260 °C for 2 h and 280 °C for 2 h to completely remove the solvent and achieve fully imidization. The chemical structure of polyimide is shown in Scheme 1 (c). The PI/MMT nanocomposites, in which the MMT was organo-modified with 1-hexadecylamine, OM-l and OM-m, were named PI/MMT-16C, PI/MMT-l and PI/MMT-m, respectively.

2.5. Characterization

^{1}H NMR spectra were recorded on a Mercury 400 MHz NMR spectrometer. Elemental analysis was conducted on an Elementar Varioel apparatus. A Perkin–Elmer Paragon 1000 infrared spectrophotometer was used to record the IR spectra of OM-l, OM-m and modified MMT (KBr). A Thermo Jawell Ash IRIS Advantage 1000 inductively coupled plasma spectrometer (ICP) was used to detect the ion exchange ratio of various modifiers. The wide angle X-ray diffraction patterns were measured on a Rigaku Geiger Flex D/max-RB diffractometer using Cu K_α radiation (40 kV, 100 mA, $\lambda = 0.154$ nm), filtered by Cr. The experiments were performed in a range of $2\theta = 1.0–35°$ with a scan rate of 4°/min. Samples for transmission electron microscopic analysis were prepared by placing small strips of sample films in epoxy resin and then cut using an ultratome and placed on a 200 mesh copper grid for analysis. The TEM investigation was performed on a JEM-100CXIITEM operating at an acceleration voltage of 100 kV. The differential scanning calorimetric (DSC) curves were recorded on a Perkin–Elmer Pyris I differential scanning calorimeter under the protection of N_2 with a heating rate of 20 °C/min. The thermal gravimetric curves were measured on a Perkin–Elmer TGA 7 under N_2 flow. The temperature range was 100–800 °C with a heating rate of 20 °C/min. The dynamic thermal analysis (DMA) of the PI and PI/MMT nanocomposite films was performed on a TA 2980 DMA. The heating rate was 5 °C/min. The coefficient of thermal expansion (CTE) of the PI and the PI/MMT nanocomposite films was also measured on a TA 2980 dynamic mechanical analyzer with a TMA mode. The film was pre-exposed at 200 °C for 20 min to eliminate the residual stress. The load on the film was 100 mN and the heating rate was 5 °C/min. A temperature range of 125–175 °C was selected to calculate the CTE. The stress-strain curves of the PI and PI/MMT nanocomposite films were recorded on an Instron-4465 universal tester at the room temperature at a drawing rate of 5 mm/min. The sorption experiments of the PI/MMT nanocomposites were carried out by the following procedure. The sample films were dried in an oven at 105 °C for 8 h, and then kept in the solvents at different temperatures for a given period of time, and blotted to remove the excessive solvent. The amount of absorbed solvent was calculated from the increase in the weight of the samples.

3. Results and discussion

3.1. Organo-modification of MMT

As previously mentioned, the organo-modification of MMT is an important step in the preparation of polymer/MMT nanocomposites and primary aliphatic amines

such as 1-hexadecylamine and its quaternary ammonium salt were commonly used organic modifiers. IR and XRD were used to verify the organic modifiers designed by us have the same efficacy as the commonly used modifiers. Fig. 1 is the IR spectra of MMT, MMT-16C, MMT-l and MMT-m. The absorption bands at 1038 and 1090 cm^{-1} were characteristic of Na-MMT (Fig. 1 (a)). After the treatment, MMT-16C exhibited the characteristic bands of C–H stretching at 2914 and 2847 cm^{-1} (Fig. 1 (b)). MMT-m exhibited the characteristic absorption bands of aromatic imide at 1780, 1713 and 1385 cm^{-1} (Fig. 1 (c)). Apart from the characteristic absorption of imide ring, MMT-m also showed the characteristic absorption of ether band at 1246 cm^{-1} (C–O–C unsymmetrical stretching) (Fig. 1 (d)). The IR results only suggested that the treated MMT contained the organic modifiers but could not give the conclusion that the molecules of organo-modifiers entered the galleries of MMT. Fig. 2 (a) is the XRD patterns of Na-MMT, MMT-l, MMT-m and MMT-16C. Table 1 listed the basal spacing of MMT calculated from the Bragg's equation. The interlayer spacing of MMT was obviously increased after the treatment with chloride salt of OM-m and OM-l from $d = 1.24$ nm for pure MMT to $d = 2.34$ nm for MMT-m and $d = 2.90$ nm for MMT-l, respectively. This suggested that organo-modifiers synthesized by us successfully intercalated between layers of MMT. More importantly, it has been widely accepted that the basal spacing of MMT treated by long-chain aliphatic amine (or ammonium salt) is decided largely by the chain length and long chain length leads to high *d*-value. Although OM-m and OM-l have much smaller long axis length than OM-16C, the MMTs treated by them exhibited higher *d*-values than that treated by OM-16C. This might be contributed to the larger space volume of benzene and imide rings and highly rigid molecular structure of OM-m and OM-l. This may also suggests that the *d*-value depends not only on the chain length but also on the rigidity of organic modifier molecules. Moreover, besides the strong diffraction peak of $2\theta = 3.04°$,

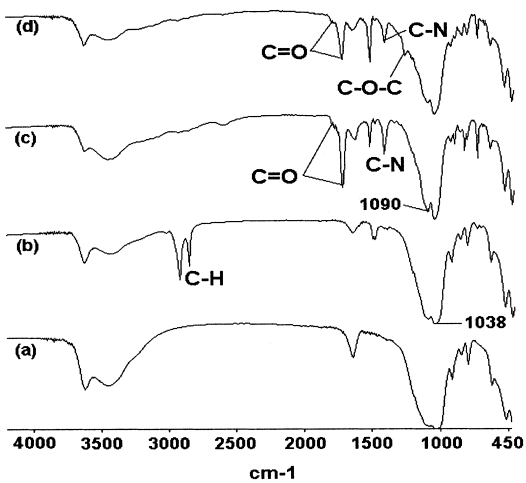

Fig. 1. IR spectra of Na-MMT, MMT-16C, MMT-l and MMT-m.

Table 1
d-Value of modified MMTs and mean value of percent recovery of sodium ions measured by ICP

Sample	2θ (deg.)	*d* (nm)	Sodium ions (wt%)	Ion exchange ratio (%)
Na-MMT	7.12	1.24	2.3860	–
MMT-16C	4.28	2.06	0.0560	97.65
MMT-m	3.78	2.34	0.0834	96.50
MMT-l	3.04	2.90	0.0417	98.25
	6.30	1.40		

a weaker diffraction peak was also observed at $2\theta = 6.30°$ for OM-l. This may indicate that the majority of MMT layers were capable of having a great amount of intercalated OM-l molecules and thus exhibited a higher *d*-value ($d = 2.90$ nm), while the minority of MMT layers were intercalated with only a small amount of OM-l molecules and exhibited a lower *d*-value ($d = 1.40$ nm). Table 1 also listed the mean value of percent recovery of sodium ions of pure MMT and organo-modified MMT measured by ICP, showing a high efficiency of the ion exchange in the OM-l and OM-m treated MMT.

3.2. Thermal stability of organo-modified MMTs

Fig. 3 were the TGA curves of organo-modified MMTs, which illustrated two or three-step degradation in the temperature range of 200–600 °C. This phenomenon was also observed and studied by Xie et al. [21] using DTA and MS. They proposed that the organics with a small molecular weight may be released first and those with a relatively high molecular weight may still exist between the interlayers until the temperature was high enough to lead to its further decomposition [21]. The initial thermal decomposition temperature (onset temperature) of MMT-16C, MMT-m and MMT-l was 252.1 °C, 320.3 °C and 344.8 °C, respectively. MMT-m and MMT-l clearly showed higher decomposition temperature compared to MMT-16C because of the higher thermal stability of OM-m and OM-l. MMT-m showed slightly lower thermal stability because of the relatively poor thermal stability of ether linkage in OM-m.

3.3. Dispersion of MMT in PI matrix

Fig. 2 (b) is the XRD patterns of MMT-l and the PI/MMT-l nanocomposite films with various MMT contents. The diffraction peak of MMT-l disappeared completely in the nanocomposites when the MMT content was below 3 wt%. This may indicate an exfoliated dispersion of MMT in PI. As the MMT content was above 4 wt%, the diffraction peak of MMT at $2\theta = 3.04°$ ($d = 2.90$ nm) disappeared and that at $2\theta = 5.30°$ ($d = 1.67$ nm)was still visible. This may indicate that the MMT layers with higher *d*-values were more favorable to the intercalation of PI molecules and the

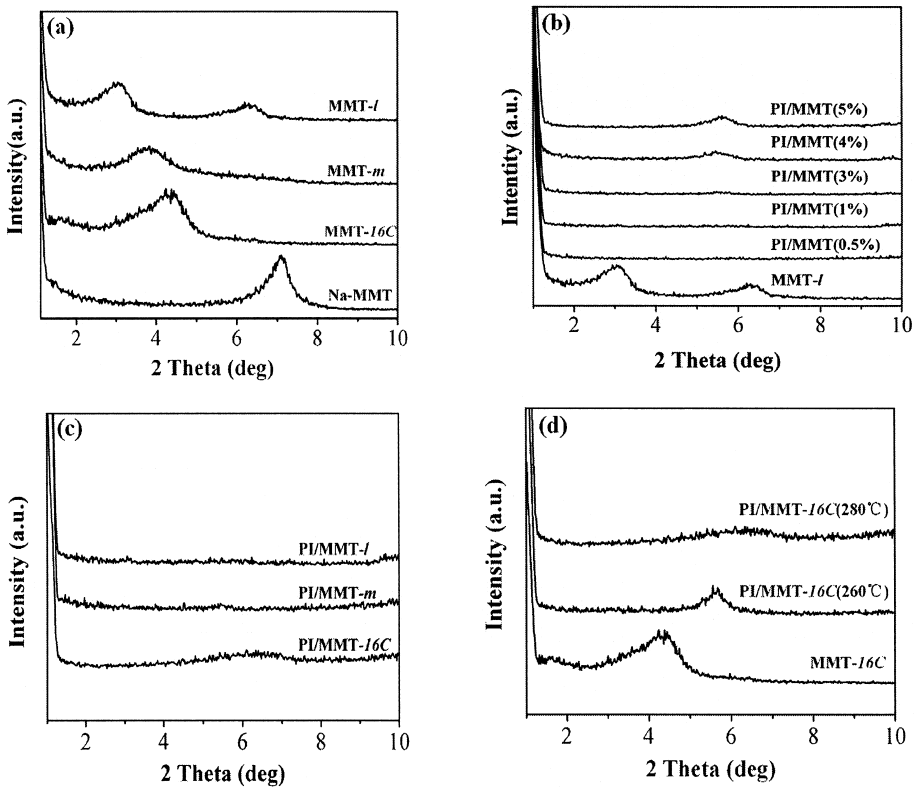

Fig. 2. XRD patterns of (a) Na-MMT and organo-modified MMTs, (b) MMT-l and PI/MMT-l nanocomposites with various MMT contents, (c) PI/MMT nanocomposites containing 3 wt% MMT, (d) MMT-16C and PI/MMT-16C nanocomposites treated at different temperature.

formation of the exfoliation morphology, while the MMT layers with lower *d*-values only increased layer spacings but were difficult to be exfoliated. This result is in good agreement with the XRD patterns of OM-l (Fig. 2 (a)). It was also found that the nanocomposite solution was clear and no obvious aggregation was observed even when the solvent was removed, also indicating the good dispersion of MMT. Fig. 4 (a) and (b) were TEM micrographs of the ultrathin-section of PI/MMT-l nanocomposite film containing 3 and 5 wt% MMT, respectively. In Fig. 4 (a), the black lines represented the intersection of the MMT layers while the grey part represented the PI matrix. The photograph indicated that MMT layers dispersed in the PI matrix in an exfoliation morphology. In Fig. 4 (b), the existence of some black agglomerate indicated the heterogeneous distribution of MMT layers in PI/MMT-l with higher clay loading.

Fig. 2 (c) showed XRD patterns of PI/MMT nanocomposites with three different organo-modified MMTs at the

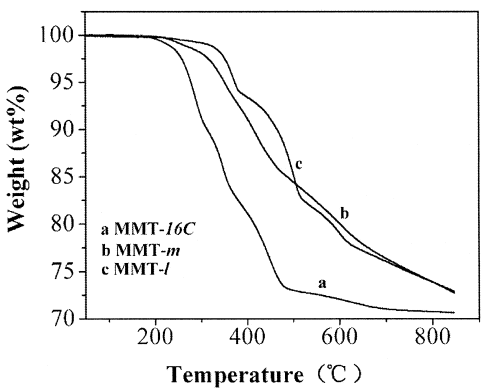

Fig. 3. TGA curves of MMT-l, MMT-m and MMT-16C.

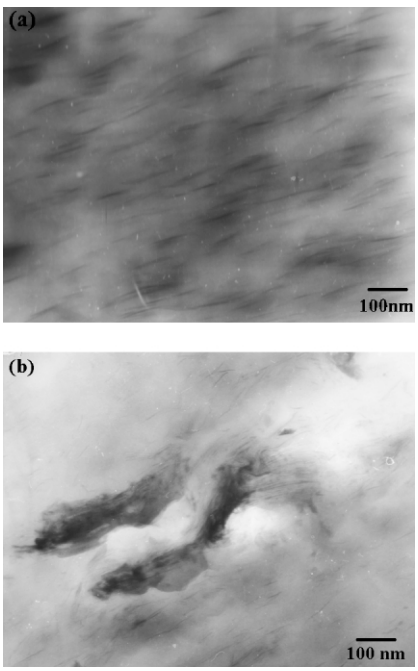

Fig. 4. TEM micrographs of the ultrathin-section of PI/MMT-l nanocomposite film containing (a) 3 wt% MMT and (b) 5 wt% MMT.

same MMT content (3 wt%). PI/MMT-16C showed a broad peak in $2\theta = 4.5–7.5°$ while the diffraction peak of MMT disappeared completely in PI/MMT-m and PI/MMT-l. It is interesting to find that the diffraction peak for MMT-16C (Fig. 2 (a) and Table 1) shifted to a higher angle (decreased layer spacing) after forming PI/MMT-16C nanocomposite. This may be caused by the lower thermal stability of OM-16C (on-set temperature at 252.1 °C, Fig. 3). Those in the MMT layers may decompose and be released when treated at 280 °C. This caused the collapse of MMT layers and the decrease in layer spacings. This can be verified by the XRD patterns of PI/MMT-16C nanocomposite treated at different temperature (Fig. 2 (d)). The diffraction peak for MMT-16C shifted to a higher angle gradually with the increase of the thermal treatment temperature and time. All these results showed that the dispersibility of MMTs treated with OM-m and OM-l was better than that of MMT treated with OM-16C. This could be contributed to the larger basal spacing of MMT-m and MMT-l, which facilitated the entrance of monomer and polymer, and also to the similar chemical structure between OM-m, OM-l and PI.

3.4. Mechanical properties of PI/MMT nanocomposites

Fig. 5 is the relationship between the MMT content and the Young's modulus of the PI/MMT nanocomposite films. The introduction of a small amount of MMT, which has a higher modulus than PI matrix, led to an obvious increase in the modulus of the nanocomposite films. When the MMT content was below 3 wt%, the Young's modulus was increased with the increase of MMT content. This quasi-linear increase in modulus may be caused by the linear increase in the number of exfoliated MMT sheets at a low MMT content. When the MMT content was further increased, the Young's modulus of the nanocomposite films leveled off or decreased slightly. This phenomenon may be caused by the aggregation of MMT in the films when the MMT content was high. Moreover, the moduli of PI/MMT-l and PI/MMT-m were higher than that of PI/MMT-16C at the same MMT content, probably caused by the better dispersion of MMT in PI/MMT-l and PI/MMT-m. This result was in good agreement with the XRD results and what observed in the dispersion of MMT in PI matrix.

The tensile strength and the elongation at break of PI/MMT nanocomposite films were shown in Fig. 6. When the MMT content was below 3 wt%, both the tensile strength and the elongation at break of PI/MMT-l, PI/MMT-m and PI/MMT-16C were increased with the increase of the MMT content. The tensile strength was increased from 113.1 MPa for PI to 164.4 MPa for PI/MMT-16C (a 45.4% increase), 168.2 MPa for PI/MMT-m (a 48.7% increase) and 182.3 MPa for PI/MMT-l (a 61.2% increase) while the elongation at break was increased from 4.5% for PI to 4.9% for PI/MMT-16C (a 8.9% increase), 6.5% for PI/MMT-m (a 44.4% increase) and 5.2% for PI/MMT-l (a 15.6% increase) nanocomposites containing 3 wt% MMT. Considering the exfoliated dispersion of MMT in PI when the MMT content was below 3 wt%, this result indicated that PI could be strengthened and toughened simultaneously by the introduction of exfoliated MMT. Firstly, the increase in the tensile strength of the PI/MMT nanocomposites could be caused by the strong interfacial interaction between MMT and PI matrix. Secondly, the large amount of interface between the exfoliated MMT sheets and PI could effectively reduce the formation of the shear zone and the layer structure of MMT could also stop the development from the shear zone to cracks. When the MMT content exceeded 3 wt%, both the tensile strength and the elongation at break were decreased probably due to the aggregation of MMT in PI matrix.

Furthermore, both the tensile strength and the elongation at break of PI/MMT-l and PI/MMT-m nanocomposites increased more distinctly than PI/MMT-16C nanocomposites. The molecules of OM-l and OM-m possess structure similar to PI, which could enhance the interfacial interaction between the layered silicates and PI matrix. Moreover, from the XRD results, the MMT sheets in PI/MMT-l and PI/MMT-m nanocomposites had better dispersibility than in PI/MMT-16C. These may be the reasons leading to the difference in the tensile strength and the elongation at break of those three types of PI/MMT nanocomposites.

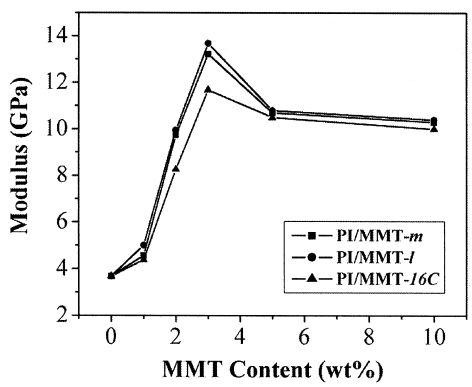

Fig. 5. Relationship between the MMT content and the Young's modulus of the PI/MMT nanocomposite films.

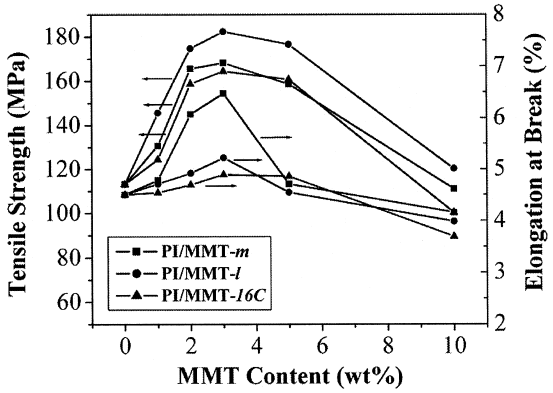

Fig. 6. Tensile strength and elongation at break of PI and PI/MMT nanocomposite films with various MMT contents.

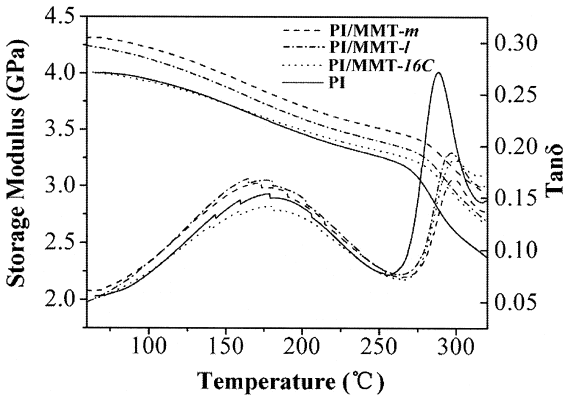

Fig. 7. DMA curves of PI and PI/MMT nanocomposite films containing 3 wt% MMT.

Fig. 7 showed the DMA curves of the PI and PI/MMT nanocomposite films containing 3 wt% MMT. The tanδ peak of nanocomposites gradually shifted to a slightly higher temperature and broadened in comparison to PI. This could be also explained by the existence of the strong interaction between MMT and PI matrix, which limited the movement of the PI chain segments. Table 2 showed the dynamic storage modulus of PI and PI/MMT nanocomposite films containing 3 wt% MMT at various temperatures and their glass transition temperatures obtained from tanδ. It was found that the storage modulus of PI below and above its T_g was increased when a small amount of MMT was introduced.

3.5. Thermal properties of PI/MMT nanocomposites

Fig. 8 (a) showed the TGA curves of PI/MMT-l nanocomposites with various MMT contents. The thermal stability of the nanocomposites was increased with increased MMT content. The on-set thermal decomposition temperature accessed by TGA was increased from 522 °C for PI to 550 °C for PI/MMT-l nanocomposite containing 5 wt% MMT. The data of Table 3 showed that the on-set thermal decomposition temperature, temperatures at 5% and 10% weight loss were increased with the increase of MMT content. MMT possessed high thermal stability and its layer structure exhibited great barrier effect to hinder the evaporation of the small molecules generated in the thermal decomposition to limit the continuous decomposition of the PI matrix.

Fig. 8 (b) showed the TGA curves of PI and PI/MMT nanocomposites with 3 wt% MMT. The on-set decomposition temperatures of PI/MMT-16C, PI/MMT-l and PI/MMT-m were 526, 547 and 549 °C, respectively, and PI/MMT-l and PI/MMT-m showed higher thermal stability than PI/MMT-16C. OM-l and OM-m contained the same imide structure as PI, and this might reinforce the synergism between the silicate sheets and the PI matrix, and resultantly, enhanced the barrier property of MMT. Another interesting phenomenon was that at the same MMT content (3 wt%) the char contents of PI/MMT-l and PI/MMT-m were higher than that of PI/MMT-16C.

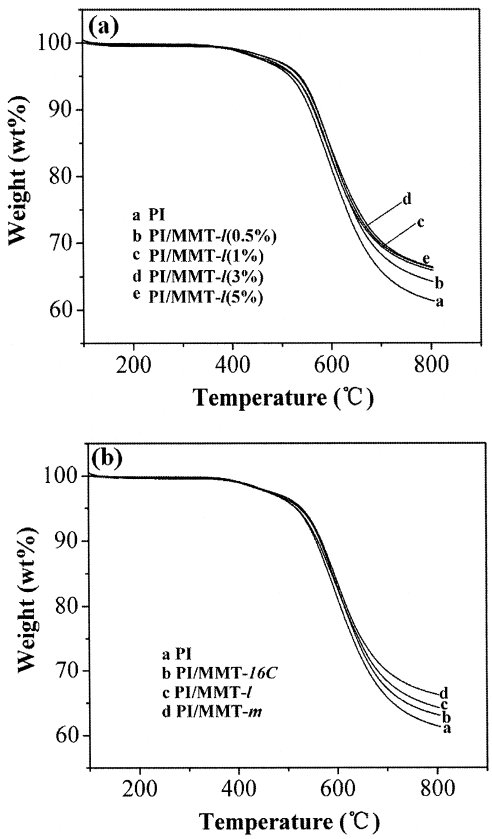

Fig. 8. TGA curves of (a) PI and PI/MMT-l nanocomposites with various MMT contents and (b) PI and PI/MMT nanocomposites containing 3 wt% MMT.

Fig. 9 (a) showed DSC traces of PI/MMT-l nanocomposites with various MMT contents. The T_g of the nanocomposites was slightly increased as the MMT content was

Table 2
Dynamic storage modulus of PI and PI/MMT nanocomposites containing 3 wt% MMT and their glass transition temperatures obtained from tan δ

Sample	Storage modulus (GPa)				Glass transition temperature[a] (°C)
	60 °C	150 °C	230 °C	310 °C	
PI	4.00	3.73	3.34	2.48	289.8
PI/MMT-16C	4.01	3.73	3.38	2.77	305.1
PI/MMT-l	4.24	3.88	3.47	2.80	300.0
PI/MMT-m	4.31	3.98	3.58	3.02	302.9

[a] The glass transition temperatures were measured at the peak tops of tan δ.

Table 3
Thermal stability of PI and PI/MMT-l nanocomposites

MMT content (wt%)	0	0.5	1	3	5
T_d (°C)[a]	522	542	541	547	550
T_5 (°C)[b]	515	524	526	533	536
T_{10} (°C)[c]	556	563	566	570	572
T_g (°C)[d]	270	273	273	275	282

[a] Thermal decomposition temperature (on-set) from TGA measurement, scan rate: 20 °C/min, N_2 protection.
[b] Temperature at 5% weight loss from TGA measurement, scan rate: 20 °C/min, N_2 protection.
[c] Temperature at 10% weight loss from TGA measurement, scan rate: 20 °C/min, N_2 protection.
[d] Obtained from DSC measurements, scan rate: 20 °C/min, N_2 protection.

increased. The T_g was increased from 270.2 °C for PI to 275.7 °C for the nanocomposite containing 3 wt% MMT and further to 282.4 °C for the nanocomposite containing 5 wt% MMT. This could be due to the strong interaction between MMT and PI, which limited the cooperative motions of the PI chain segments.

Fig. 9 (b) showed the DSC curves of different PI/MMT nanocomposites containing 3 wt% MMT. It is interesting to find that the T_g of PI/MMT-m and PI/MMT-l nanocomposites was slightly lower than that of PI/MMT-16C. As illustrated previously, PI/MMT nanocomposites were thermally treated consecutively from 70 to 280 °C. In this process, OM-16C may be decomposed and released from the nanocomposites completely because of its poor thermal stability while OM-m and OM-l may be only partially decomposed and released and some organic molecules were still trapped in PI matrix. The existence of these organic molecules may lead to the plasticization and thus slight decrease in T_g of the nanocomposites. This result was consistent with the DMA results.

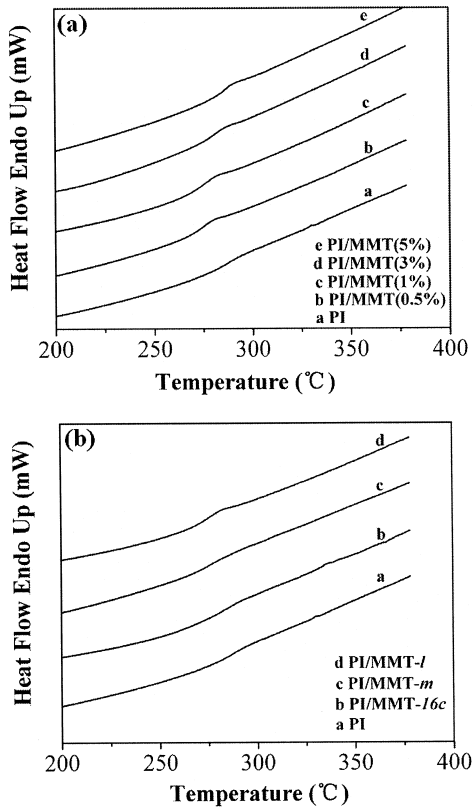

Fig. 9. DSC curves of (a) PI and PI/MMT-l nanocomposites with various MMT contents and (b) PI and PI/MMT nanocomposites containing 3 wt% MMT.

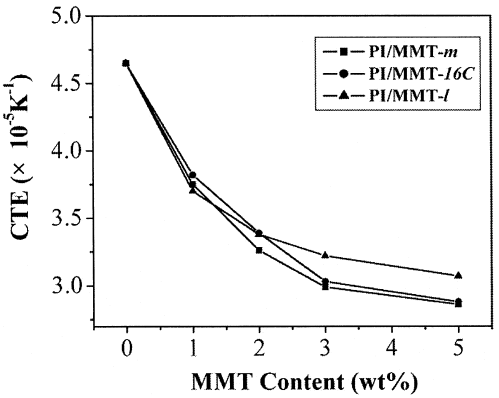

Fig. 10. Relationship between the MMT content and the coefficient of thermal expansion of the PI/MMT-l, PI/MMT-m and PI/MMT-16C nanocomposite films.

The reduced segmental movement of PI matrix with the introduction of MMT would also lead to a decrease in the coefficient of thermal expansion (CTE). Fig. 10 is the relationship between the MMT content and the CTE of the nanocomposite films. The introduction of a small amount of MMT effectively reduced the CTE. The decrease in CTE (or increase in size-stability) is extremely desired when PI is applied in microelectronic and optoelectronic fields.

3.6. Solvent resistance of PI/MMT nanocomposites

Table 4 listed the results of the solvent uptake measurement of nanocomposites with various MMT contents. Firstly, the samples were immersed in solvents at 25 °C for 24 h. However, it was observed that the solvent uptake had not reached equilibrium. So, the samples were immersed for another two days, and heated to 100 °C for 1 h aiming at investigating the solvent resistance at a relatively high temperature and the saturated solvent uptake of the PI/MMT nanocomposites. It was observed that the introduction of MMT led to an obvious decrease in the solvent uptake in both processes. For example, the water uptake ratio was decreased from 0.87% (25 °C) and 1.22% (100 °C) for PI to 0.55% (25 °C) and 0.82% (100 °C) for PI/MMT-l, 0.60% (25 °C) and 0.83% (100 °C) for PI/MMT-m, 0.61% (25 °C) and 0.86% (100 °C) for PI/MMT-16C nanocomposites contained 5 wt% MMT. The decrease in solvent uptake may be caused by hereinafter reasons. Firstly, the strong interaction between MMT and PI matrix led to the formation of 'bound polymer', polymer on close proximity to the reinforcing filler (MMT) which was either physisorbed or chemisorbed and therefore

Table 4
Solvent uptake ratios of PI, PI/MMT-l, PI/MMT-m and PI/MMT-16C nanocomposites with various MMT contents

Solvent uptake ratio (%)[a]	Water		Ethanol		Xylene	
	25 °C[b]	100 °C[c]	25 °C	100 °C	25 °C	100 °C
PI	0.87	1.22	0.42	0.46	0.70	1.42
PI/MMT-l-1%	0.80	0.92	0.08	0.20	0.68	1.22
PI/MMT-l-3%	0.68	0.81	0	0.18	0.51	1.06
PI/MMT-l-5%	0.55	0.82	0	0.18	0.42	0.90
PI/MMT-m-1%	0.82	0.90	0.22	0.40	0.62	1.28
PI/MMT-m-3%	0.63	0.77	0.18	0.33	0.58	1.07
PI/MMT-m-5%	0.60	0.83	0.12	0.20	0.46	0.88
PI/MMT-16C-1%	0.83	1.01	0.37	0.52	0.64	1.31
PI/MMT-16C-3%	0.72	0.83	0.36	0.41	0.58	1.10
PI/MMT-16C-5%	0.61	0.86	0.37	0.41	0.51	1.08

[a] The calculation formula of the solvent uptake ratio: $(W_{wet} - W_{dry})/W_{dry} \times 100\%$.
[b] The sample was soaked in solvent at 25 °C for 24 h.
[c] The sample was soaked in solvent at 25 °C for three days, 100 °C for 1 h.

restricted the solvent uptake [28]. Secondly, the large aspect ratio of MMT layers possessed excellent barrier properties, and especially the exfoliated structure of MMT layers could maximize the available surface area of the reinforcing phase. It was also found that PI/MMT-l and PI/MMT-m exhibited stronger solvent resistance than PI/MMT-16C at the same MMT content probably due to the stronger interfacial interaction between MMT-l and MMT-m and PI matrix, and better dispersibility of MMT in PI/MMT-l and PI/MMT-m. The high water uptake of the microelectronic devices by the polymers used such as epoxy and polyimide is one of the main reasons leading to their failure. Therefore the finding that the water uptake can be reduced by the introduction of MMT may extend the application of polymers in microelectronic and optoelectronic devices.

4. Conclusions

Two thermally stable, rigid-rod aromatic amines have been synthesized and used as organo-modifiers for MMT. The MMT treated by them exhibited higher basal spacings than that treated by 1-hexadecylamine. The MMT layers were basically exfoliated in the PI/MMT nanocomposites prepared by in-situ polymerization when the MMT content was below 3 wt%. The MMT content influenced the properties of PI/MMT nanocomposites significantly. When the MMT content was below 3 wt%, the PI/MMT nanocomposites were strengthened and toughened at the same time. The introduction of a small amount of MMT also led to improvement in thermal stability, slight increase in glass transition temperature, marked decrease in coefficient of thermal expansion and decrease in solvent uptake. PI/MMT-l and PI/MMT-m exhibited better mechanical, thermal and solvent resistance properties than PI/MMT-16C probably due to the similar molecular structure of OM-l and OM-m with PI and much stronger interfacial interaction between MMT and PI matrix.

Acknowledgements

The authors would like to thank the Ministry of Education of China (Kuashiji Scholars' Project) and Science and Technology Commission of Shanghai Municipal Government (Nano-Project) for their financial support.

References

[1] Giannelis EP, Krishnamoorti R, Manias E. Adv Polym Sci 1999;138:107.
[2] Vaia RA, Jandt KD, Kramer EJ, Giannelis EP. Macromolecules 1995;28:8080.
[3] Vaia RA, Giannelis EP. Macromolecules 1997;30:7990.
[4] Manias E, Touny A, Wu L, Strawhecker K, Lu B, Chung TC. Chem Mater 2001;13:3516.
[5] LeBaron PC, Pinnavaia TJ. Chem Mater 2001;13:3760.
[6] Choi YS, Choi MH, Wang KH, Kim SO, Kim YK, Chung IJ. Macromolecules 2001;34:8978.
[7] Liu X, Wu Q. Polymer 2001;42:10013.
[8] Bharadwaj RK. Macromolecules 2001;34:9189.
[9] Alexandre M, Beyer G, Henrist C, Cloots R, Rulmont A, Jérôme R, Dubois P. Chem Mater 2001;13:3830.
[10] Fong H, Vaia RA, Sanders JH, Lincoln D, Vreugdenhil AJ, Liu W, Bultman J, Chen C. Chem Mater 2001;13:4123.
[11] Chen TK, Tien YI, Wei KH. J Polym Sci Part A: Polym Chem 1999;37:2225.
[12] Byun HY, Choi MH, Chung IJ. Chem Mater 2001;13:4221.
[13] Messersmith PB, Giannelis EP. J Polym Sci Part A: Polym Chem 1995;33:1047.
[14] Solomon MJ, Almusallam AS, Seefeldt KF, Somwangthanaroj A, Varadan P. Macromolecules 2001;34:1864.
[15] Huang X, Lewis S, Brittain WJ. Macromolecules 2000;33:2000.
[16] Yoon JT, Jo WH, Lee MS, Ko MB. Polymer 2001;42:329.
[17] Agag T, Koga T, Takeichi T. Polymer 2001;42:3399.
[18] Huang JC, Zhu ZK, Ma XD, Qian XF, Yin J. J Mater Sci 2001;36:871.
[19] Vaia RA, Giannelis EP. Macromolecules 1997;30:8000.
[20] Xie W, Gao Z, Pan WP, Hunter D, Singh A, Vaia R. Chem Mater 2001;13:2979.
[21] Xie W, Gao Z, Liu K, Pan WP, Vaia R, Hunter D, Singh A. Thermochim Acta 2001;367–368:339.
[22] Delozier DM, Orwoll RA, Cahoon JF, Johnston NJ, Smith Jr. JG, Connell JW. Polymer 2002;43:813.
[23] Liu H, Kim DW, Blumstein A, Kumar J, Tripathy SK. Chem Mater 2001;13:2756.
[24] Huang JC, Zhu ZK, Qian XF, Yin J, Sun YY. Polymer 2001;42:873.
[25] Yang Y, Zhu Z, Yin J, Wang X, Qi Z. Polymer 1999;40:4407.
[26] Fu X, Qutubuddin S. Mater Lett 2000;42:12.
[27] Fu X, Qutubuddin S. Polymer 2001;42:807.
[28] Kraus GJ. J Appl Polym Sci 1963;7:861.
[29] Hasegawa M, Horie K. Prog Polym Sci 2001;26:259.
[30] Yano K, Usuki A, Okada A, Kurauchi T, Kamigaito O. J Polym Sci Part A: Polym Chem 1993;31:2493.
[31] Yano K, Usuki A, Okada A. J Polym Sci Part A: Polym Chem 1997;35:2289.